Colloids and Surfaces A: Physicochemical and Engineering Aspects 691 (2024) 133857

Contents lists available at ScienceDirect

Colloids and Surfaces A: Physicochemical and Engineering Aspects

journal homepage: www.elsevier.com/locate/colsurfa

Effective recovery of phosphate from wastewater using biodegradable calcium-rich shell wastes composite macroporous cryogel

Satabodee Kaewnoo [a], Worawit Wongniramaikul [a], Chanita Boonkanon [a], Tarawee Taweekarn [a], Bussakorn Kleangklao [a], Somsak Limwongsakorn [b], Chanadda Phawachalotorn [c], Diana S. Aga [d], Aree Choodum [a,*]

[a] Integrated Science and Technology Research Center, Faculty of Technology and Environment, Prince of Songkla University, Phuket Campus, Kathu, Phuket 83120, Thailand
[b] Department of Industrial Technology, Faculty of Science and Technology, Phuket Rajabhat University, Muang, Phuket 83000, Thailand
[c] King Mongkut's Institute of Technology Ladkrabang, Prince of Chumphon Campus, Chumphon 86160, Thailand
[d] Department of Chemistry, University at Buffalo, The State University of New York, Buffalo, NY 14260, United States

HIGHLIGHTS

- Oyster shell waste was used to prepare a green calcium-rich adsorbent.
- It was crushed, calcined, and composited with starch gel making a calcium-rich tablet.
- A calcium-rich tablet (Cry−Ca−COS) can be used for phosphate removal and recovery.
- Cry−Ca−COS can remove phosphate from real samples indicating great applicability.
- The used material can be biodegraded within 24 days under soil burial conditions.

GRAPHICAL ABSTRACT

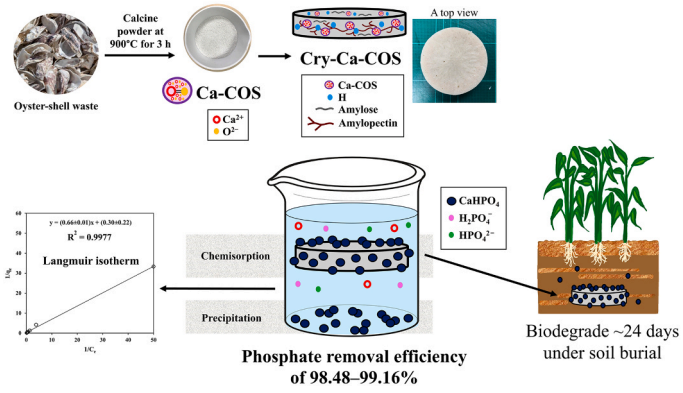

ARTICLE INFO

Keywords:
Phosphate recovery
Biocryogel
Calcium-rich calcined oyster shell
Composite
Phosphate removal
Adsorption

ABSTRACT

The recovery of phosphorus from wastewater holds promise as a sustainable source of organic phosphorus for agricultural use while aiding in meeting legislative discharge limits for phosphorus to control and mitigate eutrophication. This study introduces a novel approach in which calcium-rich calcined oyster shell (Ca–COS) is immobilized on a starch-based monolithic cryogel, resulting in a green tablet (Cry–Ca–COS) capable of efficiently recovering phosphate from water through chemisorption on the material surface and precipitation in the liquid phase. The formed tablet prevents sorbent loss post-adsorption, facilitating reusability. Under optimal conditions (i.e., three 0.83 cm thick Cry–Ca–COS tablets, an initial phosphate concentration of 12 mg L^{-1} in 1 L without pH adjustment (pH 6.3), and a contact time of 60 minutes), a phosphate removal efficiency of 83.11% ± 0.68% and a maximum removal capacity of 9.97 mg g^{-1} were achieved. Both the Langmuir isotherm model and pseudo-second-order kinetic model exhibited good fits to the experimental data, with an estimated activation energy

* Corresponding author.
E-mail address: aree.c@phuket.psu.ac.th (A. Choodum).

https://doi.org/10.1016/j.colsurfa.2024.133857
Received 25 January 2024; Received in revised form 15 March 2024; Accepted 29 March 2024
Available online 30 March 2024

of 81.9 kJ mol^{-1} and a positive enthalpy of 9.3 kJ mol^{-1}, indicating an endothermic chemisorption process with a monolayer surface coverage of phosphate on Cry–Ca–COS. In real samples, Cry–Ca–COS demonstrated a high removal efficiency ranging from 98.48% ± 1.87%–99.16% ± 0.72%, with the adsorbed material biodegrading within 24 days under soil burial conditions. A preliminary study was conducted to explore the feasibility of utilizing phosphate-adsorbed Cry–Ca–COS as a fertilizer for cultivating water spinach (*Ipomoea aquatica* Forsk.), and further in-depth investigation is required for a comprehensive report in the future. Thus, Cry–Ca–COS emerges as an environmentally friendly and effective tool for phosphate removal and recovery.

1. Introduction

Phosphorus is vital for food production as a primary macronutrient for plant growth, widely utilized in chemical fertilizers. With fertilizer production currently relying on nonrenewable phosphate rock (85% of 14.2 million tons per year), primarily sourced from limited regions like Morocco and Western Sahara, there is a looming global challenge for food security [1–4]. These resources may be depleted in the next 30–200 years [4–7]. Recovering phosphorus from wastewater, especially in municipal treatment, is gaining interest as it contains vital phosphorus. If not recovered, this phosphorus can contribute to ocean pollution and eutrophication, especially in the form of phosphate [8]. Elevated phosphate concentrations surpassing 0.02 mg L^{-1} can induce eutrophication, a critical environmental issue associated with adverse effects on mollusks, fish, and other aquatic species [9,10]. Algal growth may lead to pipe and turbine blockages, and the presence of toxic algae and dinoflagellates can pose health risks and disrupt economies [11,12]. Therefore, phosphate removal from water bodies is imperative for mitigating and controlling eutrophication.

Adsorption proves to be an appealing method applicable for the removal of phosphorus from wastewater, offering the possibility of simultaneous phosphorus recovery. This method boasts simplicity in operation, high removal efficiency, and cost-effectiveness [9,11–14]. A variety of adsorbents have been employed in phosphate removal, including carbonaceous sorbents like biochar [11,12], calcium-based materials such as calcium silicate hydrate [15–17], and calcium hydroxide [18]. Additionally, natural waste like eggshells, crab shells, and oyster shells [19,20], along with industrial byproducts like steel slag [21] and other industrial wastes [14], represent low-cost materials with the potential for application in the development of a cost-effective phosphate removal and recovery process.

Oyster shells are abundantly available on the seashores of many countries, including Thailand [22]. However, their waste production has increased significantly due to rising consumption and production [19], leading to disposal problems. These shells contain a high calcium content (approximately 96% as $CaCO_3$) [22,23] and can serve as a rich source of calcium carbonate adsorbent. This utilization can effectively alkalize wastewater, offering an economical alternative to using chemically produced calcium carbonate in the wastewater treatment process [24]. The oyster shell powder (24 g), produced using high-pressure steam to achieve a particle size of 200 μm and a surface area of 237 m^2 g^{-1} , can reduce phosphate concentration from 50 mg L^{-1} to 7 mg L^{-1} in 7.7 days within a 1 L solution [24]. Crushed oyster shells can also serve as adsorption and filtration media for phosphorus removal [25,26] and can be integrated into constructed wetlands, exhibiting a phosphorus adsorption capacity of 16 g kg^{-1} [22,27]. However, the constructed wetland unit primarily contributes to the treatment performance [22]. Additionally, calcining oyster shells has been shown to enhance their efficiency in phosphorus removal [19,28,29].

All the above studies have used fine powder and/or particles to adsorb phosphate because a smaller particle size increases the active surface area, which results in a greater removal capacity. However, this comes with the tradeoff of loss of the adsorbent material during the removal process, which decreases its utilization efficiency and pollutes the environment [13,16,30]. Some studies have attempted immobilizing these adsorptive materials on polymeric supports such as polyvinyl alcohol (PVA) [13]. However, PVA is a synthetic petroleum-based polymer, which is not environmentally friendly. Opting for a naturally occurring polymer could be a more environmentally friendly choice. Recently, a starch-based cryogel composite incorporating calcium silicate hydrate (CSH) was created, showcasing notable efficiency in phosphate removal [16]. However, it's worth noting that the resulting

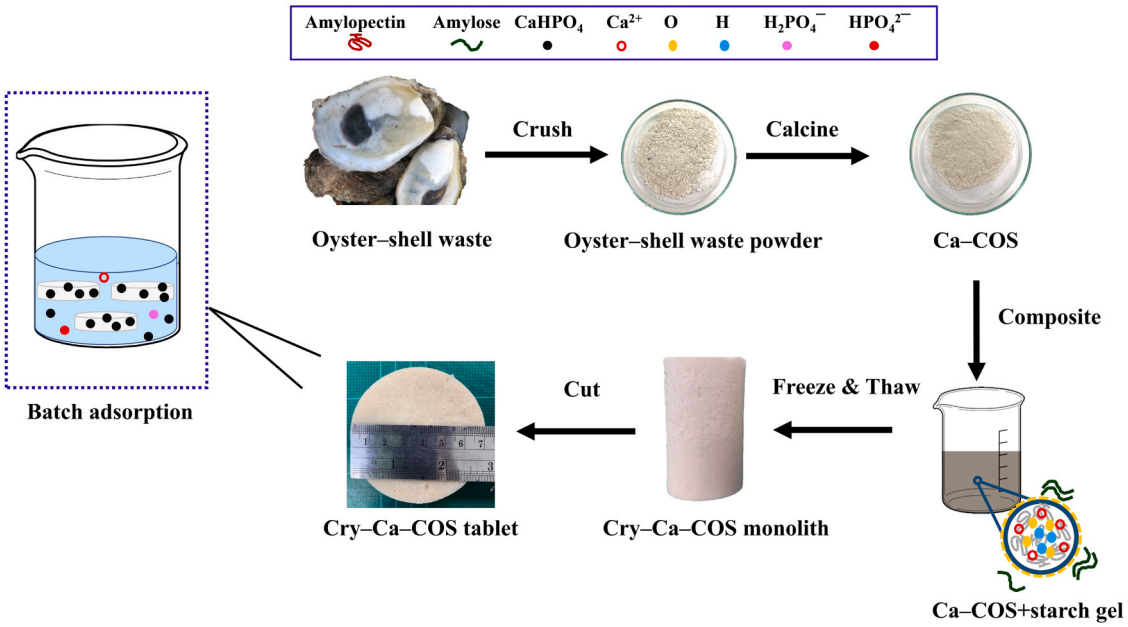

Fig. 1. Preparation of calcium-rich calcined oyster shell (Ca–COS) composite starch cryogel (Cry–Ca–COS).

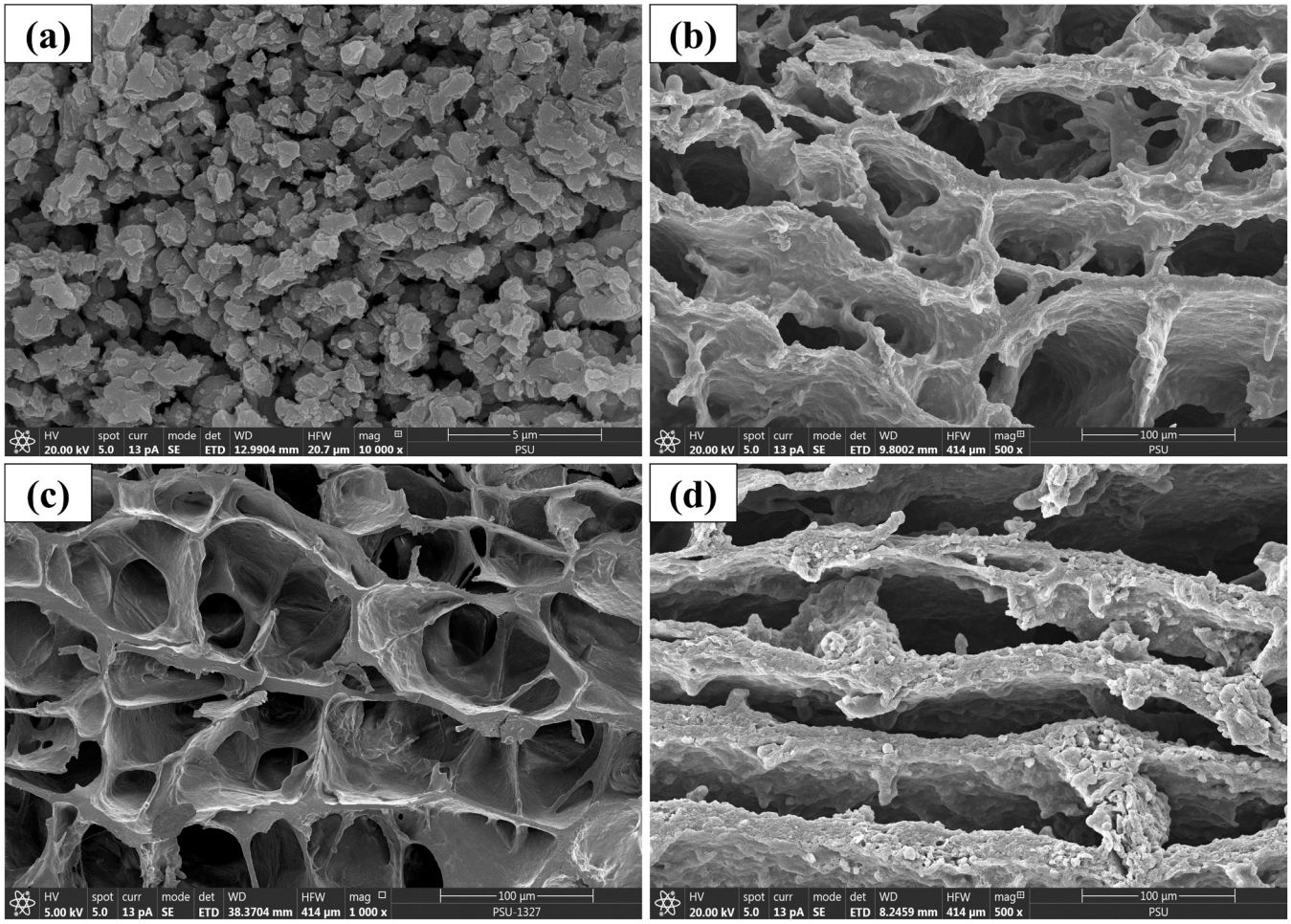

Fig. 2. FESEM images of (a) Ca–COS, (b) Cry–Ca–COS, (c) Cry, and (d) Cry–Ca–COS after phosphate adsorption.

material still relies on synthesized CSH.

In this study, oyster shell waste was repurposed into a calcium-rich calcined biomaterial, which was then combined with a starch-based monolithic cryogel to create an environmentally friendly adsorbent for phosphate removal and recovery. Calcium-rich calcined powder derived from oyster shell waste (Ca–COS) has been immobilized within a starch cryogel network to create a novel green adsorptive tablet for phosphate (Cry–Ca–COS). This innovative tablet aims to minimize the loss of Ca–COS during the removal process and facilitate the recovery of the adsorbent after use. Batch experiments were conducted using both synthetic samples and real water samples containing phosphate to assess the adsorption mechanism, kinetics of the developed composite, and phosphate removal efficiency. The biodegradability of the novel green tablet after phosphate adsorption was also investigated, along with its potential use as fertilizer for cultivating water spinach (*Ipomoea aquatica* Forsk.). Therefore, this work not only utilizes waste to develop a novel green adsorbent tablet for phosphate removal to prevent water pollution but also aligns with the zero-waste concept, leaving no waste after use.

2. Materials and methods

2.1. Materials

The description of all materials utilized in this work can be found in Supplementary Material S1.

2.2. Preparation of adsorbents

Oyster shell waste was cleaned to remove sediment and other debris before drying by exposure to the sun. The oyster shells were then crushed and sieved to obtain a particle size of $\leq$0.125 mm (120 mesh). The crushed powder was then calcined in an air atmosphere at 900°C for 3 hours to obtain calcium-rich calcined oyster shell (Ca–COS), which was stored in a desiccator for further use. A starch cryogel (Cry) was produced using the freeze and thaw technique, as previously reported [16]. Further details can be found in Supplementary Data S2. A Ca–COS composited starch cryogel (Cry–Ca–COS) was prepared using the same procedure as Cry, with the addition of Ca–COS (2.5–75 g) to the starch gel (500 g). The resulting Cry–Ca–COS was cut into small pieces with a length of 2.5 cm, dried, and stored in a zip-locked plastic bag for further use. Fig. 1 illustrates the preparation of Cry–Ca–COS by combining Ca–COS with a starch-based monolithic cryogel.

2.3. Characterization of adsorbents

The characterization of the adsorbent is detailed in Supplementary Material S3.

2.4. Adsorption experiments and models

Experiments were conducted to explore the phosphate adsorption capabilities of Ca–COS and Cry–Ca–COS using a modified batch adsorption method derived from literature procedures [9,10,16]. The dosages of Ca–COS and Cry–Ca–COS adsorbents were optimized and

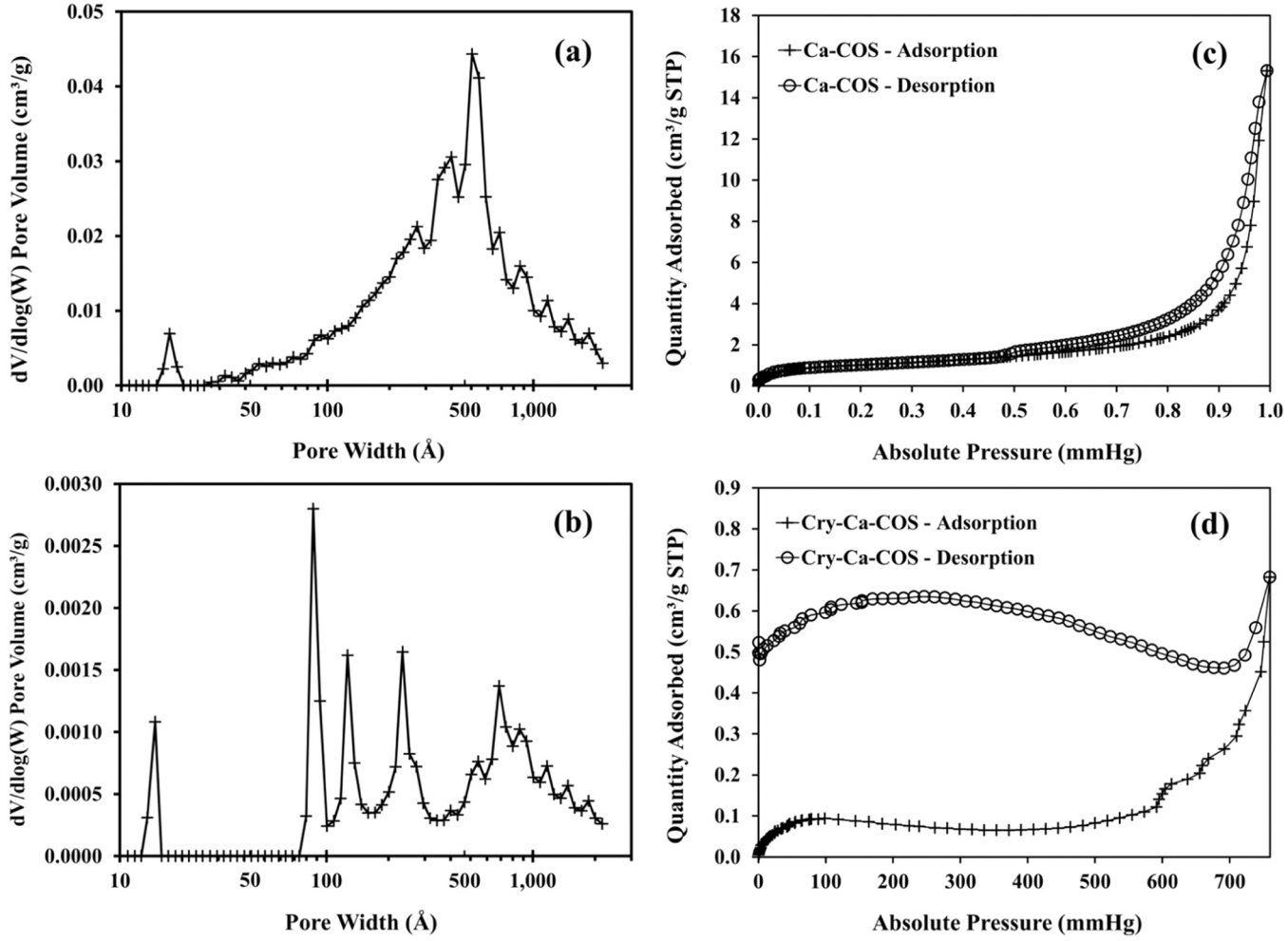

Fig. 3. (a, b) Pore size distributions and (c, d) Nitrogen adsorption isotherms of Ca–COS (top row) and Cry–Ca–COS (bottom row).

maintained throughout the adsorption experiments. Various doses of Ca–COS (0.5, 1, 2.5, 5, 10, 15 g) was added to a 12 mg L^{-1} phosphate solution without pH adjustment (1 L, pH = 6.3) shaken at 150 rpm at room temperature (25°C) for 1 hour. Simultaneously, 10 g of Cry–Ca–COS tablet with varying amounts of Ca–COS (0.5, 1, 2.5, 5, 10, 15% w/w) was tested under the same conditions.

The phosphate adsorption isotherm of each material was studied by suspending optimal dosages of each material in a 1 L phosphate solution with initial concentrations ranging from 0.5 to 20 mg L^{-1}. The optimum initial concentration was then used to investigate the kinetics based on contact time (0–1440 minutes), pH (5–9), and temperature (by employing a water bath to continuously maintain the solution temperature 25°C–40°C). The solutions from each experimental condition were collected at predetermined intervals, filtered using a 0.20 μm cellulose acetate membrane, and the remaining phosphate concentrations were analyzed using the standard ascorbic acid–spectrophotometric method [31]. The amount of adsorbed phosphate at time t (Qt: mg g^{-1}) was calculated using Equation (1) (refer to supplementary data Table S1), while the removal efficiency (RE: %) was calculated using Equation (2). A blank control solution (without adsorbent) underwent the same treatment manner, and each experiment was conducted in triplicate where the average value was considered a single data point for plotting any relationships. A calibration curve was established by analyzing a series of phosphate standard solutions with concentrations ranging from 0 to 20 mg L^{-1} where the daily re-calibration was performed to ensure measurement accuracy.

The adsorption data obtained from the experiments were analyzed and fitted to kinetic adsorption models to determine the removal capacity and rate-limiting step of phosphate adsorption on Cry–Ca–COS. This includes the pseudo-first-order and pseudo-second-order models [32], employing Equations (3) to (6) explained in Table S1. The phosphate adsorption isotherm of Cry–Ca–COS was also investigated to elucidate the adsorption mechanism. The analyzed experimental data obtained from experiments at various initial concentrations were fitted to widely used isotherm models, namely Langmuir (Equations (7) to (8)) and Freundlich (Equations (9) to (10)) isotherm models [9,10,16,33,34]. Thermodynamics were investigated to examine the effect of temperature on the adsorption of phosphate on Cry–Ca–COS. Experiments were conducted to estimate changes in thermodynamic factors, including the standard Gibbs free energy change (ΔG°), enthalpy (ΔH°), and entropy (ΔS). ΔG° is given by Equations (11) and (12), while ΔH° and ΔS° are calculated using Equations (13) and (14).

3. Results and discussion

3.1. Characterization of Cry–Ca–COS

FESEM images of the prepared Ca–COS revealed agglomerated crystal particles (Fig. 2a), resembling those reported from pyrolyzed eggshells [20]. In Cry–Ca–COS, the Ca–COS particles were entrapped within the cryogel wall, leading to thicker walls and a rougher surface (Fig. 2b) compared to Cry alone (Fig. 2c). The morphology of Cry–Ca–COS comprised macropores with a large pore volume and an interconnected polymerization network, characteristic of cryogels [16,

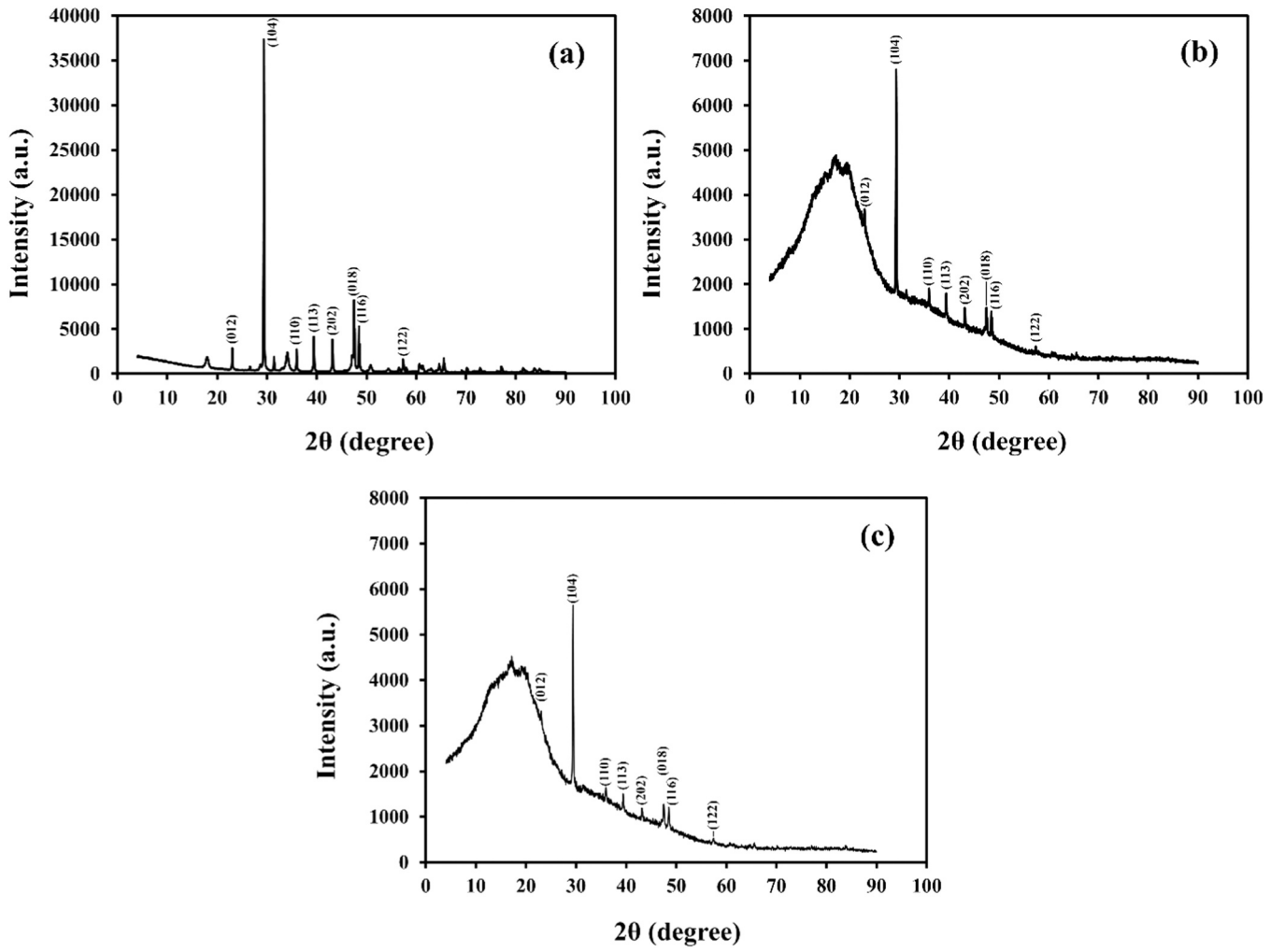

Fig. 4. XRD patterns of (a) Ca–COS and (b) Cry–Ca–COS (c) Cry–Ca–COS after phosphate adsorption.

35–37], facilitating access by adsorbates [13]. Following phosphate adsorption, Cry–Ca–COS exhibited thicker walls (Fig. 2d) with small clusters of numerous crystals on its surface, indicating a physicochemical reaction with phosphate ions.

BET analysis revealed that Ca–COS possessed a specific surface area (S_{BET}) of 3.597 m^2 g^{-1}, a total pore volume of 0.022 mL g^{-1}, and an average pore diameter of 24.44 nm. Notably, Ca–COS exhibited a greater S_{BET}, total pore volume, and average pore diameter compared to pyrolyzed eggshells, which measured 2.96 m^2 g^{-1}, 0.0076 mL g^{-1}, and 10.25 nm, respectively [20]. In contrast, Cry–Ca–COS displayed a smaller S_{BET} of 0.389 m^2 g^{-1}, a pore volume of 0.001 mL g^{-1}, and an average pore diameter of 9.65 nm. These findings align closely with those reported in previous studies, which attribute such characteristics to the entrapment of fine particles within the polymer matrix [13,16]. The reduced average pore diameter of Cry–Ca–COS suggests potential disturbance in the porous structure of Ca–COS due to immobilization in the starch gel. However, the pore distributions of Ca–COS (Fig. 3a) and Cry–Ca–COS (Fig. 3b) were similar, ranging from 5–200 nm and 9–200 nm, respectively, indicating the presence of both mesopores and macropores in both materials. Both Ca–COS and Cry–Ca–COS exhibited typical type IV isotherms with H3 hysteresis loops (Figs. 3c and 3d, respectively), signifying the presence of mesopores with a very wide pore size distribution [38]. This characteristic could facilitate the accessibility of phosphate to reach active sites, enhancing the materials' adsorption capabilities.

The XRD pattern of Ca–COS (Fig. 4a) exhibited sharp peaks at 23.0°, 29.4°, 36.0°, 39.4°, 43.1°, 47.6°, 48.5°, and 57.3° 2θ, corresponding to the (012), (104), (110), (113), (202), (018), (116), and (122) planes, respectively. These peaks are characteristic of $CaCO_3$ (JCPDS file no. 83–0577 [39]), as reported in the literature for both raw and pyrolyzed materials [16,17,39–41]. Additional peaks at 54.3°, 64.7°, and 65.6° 2θ correspond to the (220), (311), and (222) planes, respectively, of the calcium oxide phase (JCPDS file no. 78–0649) [39–41]. These findings indicate that Ca–COS contains various calcium species, potentially enhancing its phosphate removal capacity. These characteristic peaks persisted in Cry–Ca–COS (Fig. 4b) but at lower intensities. Additionally, a broad hump centered at 2θ ~20° was observed, indicative of the amorphous structure of the starch cryogel. This result suggests that the in-plane organization of the calcium atoms in Cry–Ca–COS remained the same as that in Ca–COS, implying no significant effect from the incorporation of cryogel into Ca–COS. All characteristic peaks of Ca–COS and starch in Cry–Ca–COS remained in their positions after phosphate adsorption (Fig. 4c), similar to the results observed with phosphate adsorption onto pyrolyzed eggshell [20].

The FTIR spectrum of Ca–COS (Fig. 5a) revealed absorption bands at 875, 1421, 1799, 2512, and 2919 cm^{-1}, attributed to $CaCO_3$ molecules [20]. These bands were also observed in non-pyrolyzed oyster shell waste powder (NOS) at a higher intensity (Fig. 5b), indicating a greater amount of $CaCO_3$ molecules in NOS. However, these bands shifted and decreased in intensity for Cry–Ca–COS (Fig. 5c) due to overlapping with other absorption bands from starch molecules. The peak at 712 cm^{-1}, attributed to the vibration of Ca–O bonding, was observed in both

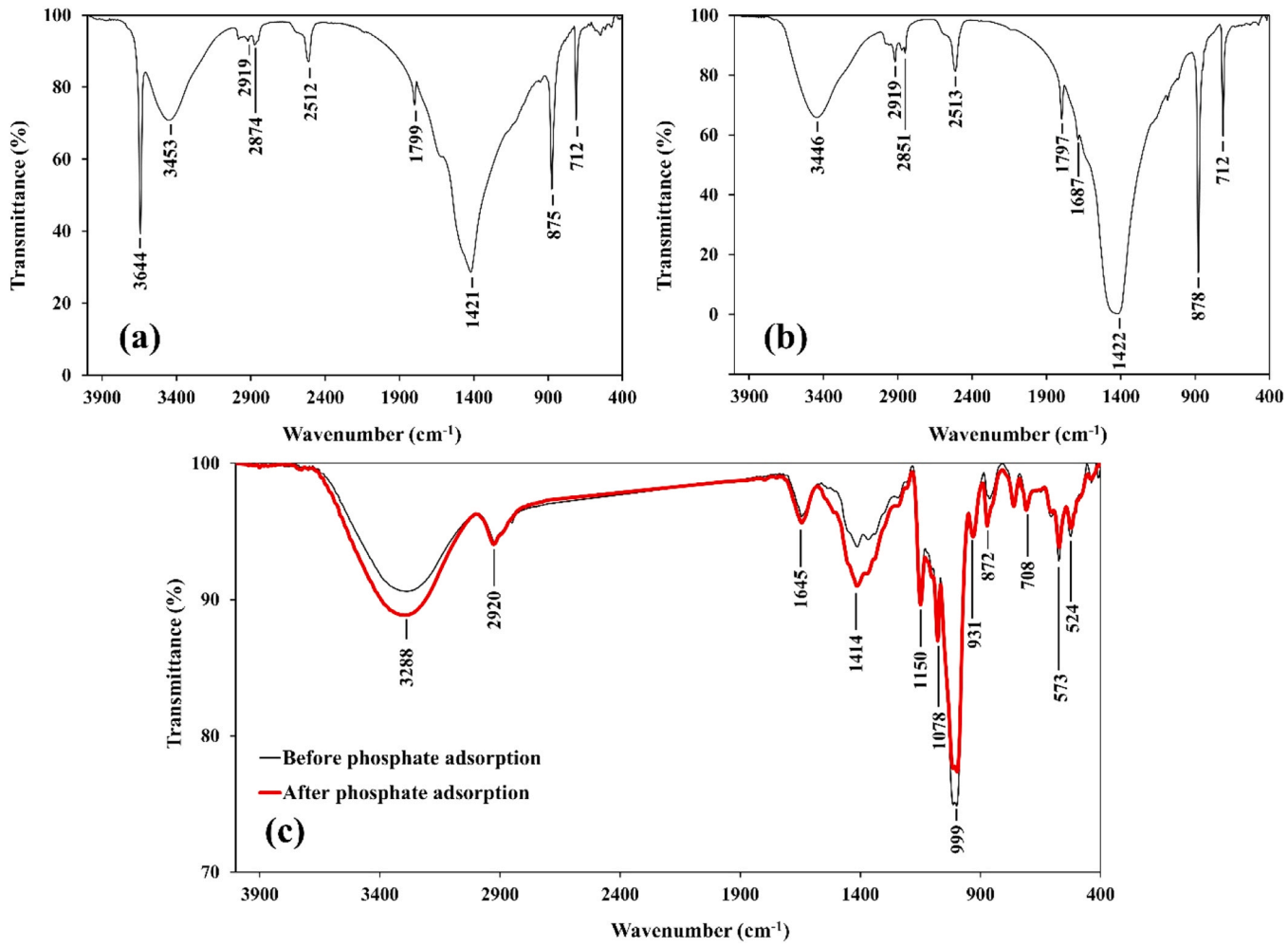

Fig. 5. FTIR spectra of (a) Ca–COS, (b) non-pyrolyzed oyster shell waste powder (NOS), and (c) Cry–Ca–COS before and after phosphate adsorption.

Ca–COS and NOS. Although commonly observed after heating $CaCO_3$-containing materials such as eggshells [20] and lime sludge [42], this band slightly shift for Cry–Ca–COS, indicating the presence of Ca–O bonding. The absorption band at 3644 cm^{-1} in Ca–COS was attributed to $Ca(OH)_2$ [20], potentially formed from the adsorption of CaO with H_2O. However, this compound was absent in NOS and Cry–Ca–COS. Since lime water was used as the cross-linker for cryogel preparation, the formed $Ca(OH)_2$ in Ca-COS may cross-link with starch molecules, resulting in the disappearance of this peak in Cry–Ca–COS. In the Cry–Ca–COS spectrum, a broad absorption band ~3300 cm^{-1} was attributed to O–H stretching from hydroxyl groups in starch molecules [16,35], overlapping with hydroxyl groups from Ca–COS at 3453 cm^{-1}. The absorption band at 1645 cm^{-1} in Cry–Ca–COS was attributed to C–O bending in amylopectin of starch molecules [16,35,43], which may overlap with the O–H bending vibrations of adsorbed water [44]. The absorption peaks at 2920 cm^{-1} and 1150 cm^{-1} in Cry–Ca–COS were attributed to C–H stretching and C–O–C vibrations in glycosidic linkage in starch molecules, respectively [16,35,43]. The vibration of C–O bonding in amylopectin, commonly present in starch cryogels [16,35,43], was also observed as intense peaks from 1078 cm^{-1} to 931 cm^{-1} in the Cry–Ca–COS spectrum, with the maximum absorbance at ~1000 cm^{-1}. This peak may overlap with the vibration of the CO_3^{2-} and PO_4^{3-} groups from the natural base composition of the bio-shell adsorbent. The stretching vibration of CO_3^{2-} has been reportedly observed at 1063 cm^{-1} in eggshell adsorbent [20], while the P–O vibration is observed at 963 cm^{-1} and within the range of 1000–1100 cm^{-1} [45,46]. The presence of absorption peaks at 483 cm^{-1} (corresponding to O–P–O bending), 573 cm^{-1} and 606 cm^{-1} (related to O–P–O asymmetric and symmetric deformation, respectively) indicates the presence of phosphate vibration [45–48] within Cry–Ca–COS. These findings suggest the potential existence of a small amount of phosphate, likely originating from the oyster shell material. After phosphate adsorption, all vibration peaks of Cry–Ca–COS remained in their positions with some changes in intensity (Fig. 5c-red line). A significant increase in the intensity of the O–H stretching from hydroxyl groups around 3300 cm^{-1} may be attributed to the additional vibration from the O–H group of the adsorbed phosphate product, such as hydroxyapatite ($Ca_{10}(PO_4)_6(OH)_2$), which has been reportedly observed between 3570 and 3420 cm^{-1} [49]. Similar to the peak at 872 cm^{-1}, which is commonly attributed to the C–O stretching from the CO_3^{2-} group [45] contained in Cry–Ca–COS, the increase in its intensity may be attributed to the additional vibration of the hydrogenophosphate (HPO_4^{2-}) groups adsorbed on the material [45,46]. It has been reported that the presence of HPO_4^{2-} groups can indicate the formation of calcium-deficient apatite phases ($Ca_{10-x}(HPO_4)_x(PO_4)_{6-x}(OH)_{2-x}$) [46]. The increasing in the CO_3^{2-} absorption band at 1414 cm^{-1} in the material after phosphate adsorption may contribute to the occurring of carbonate substitute hydroxyapatite [45,47,48] due to the dissolved carbon dioxide in the solution [47]. However, discussing the form of the phosphate product after adsorption on Cry–Ca–COS is challenging due to the presence of strong absorption peaks from the starch molecules at the same wavenumber as phosphate, as well as some bio-phosphate contained in the oyster shell.

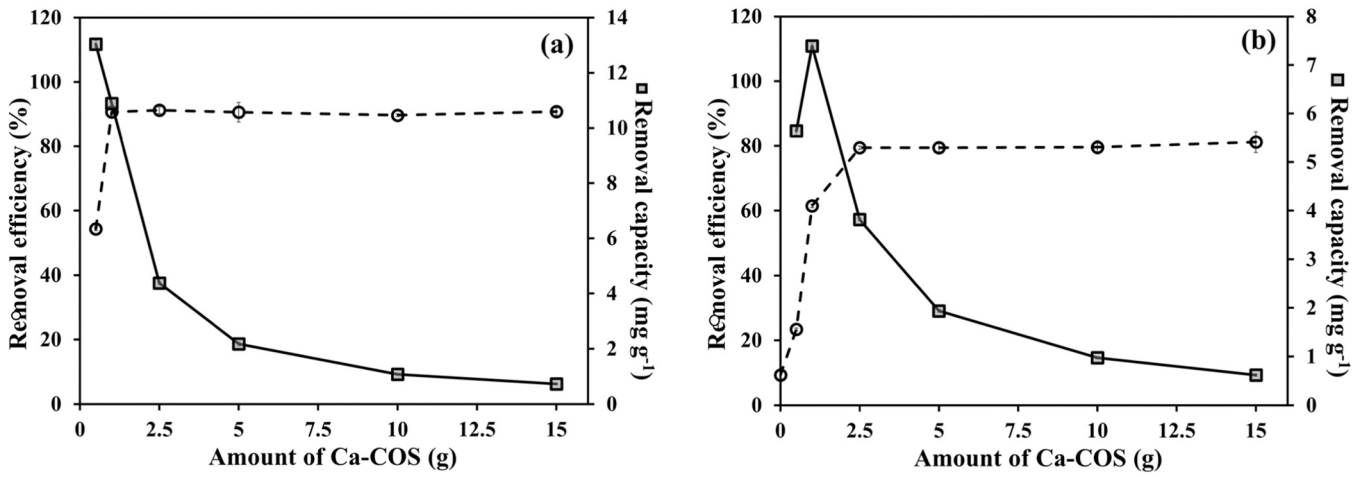

Fig. 6. Influences of the (a) amount of Ca–COS, (b) amount of Ca–COS in Cry–Ca–COS on the phosphate removal efficiency (%) and removal capacity. Conditions: phosphate concentration 12 mg L^{-1} for 1 L, without pH adjustment (pH 6.3), contact time 1 hour, temperature 25°C.

The materials before and after phosphate adsorption were analyzed by X-ray Fluorescence (XRF) to confirm the presence of the phosphate product post-adsorption. The significant increase in the amount of P_2O_5 in the material after phosphate adsorption (from 0.083% to 0.335% w/w, 4-fold as shown in Table S2) confirms the adsorption of phosphate onto the Cry–Ca–COS. It's noteworthy that there is a small amount of P_2O_5 present in Cry–Ca–COS before adsorption (0.083% w/w), indicating the initial presence of phosphate. This result aligns well with the presence of phosphate vibration peaks (at 483 cm^{-1}, 573 cm^{-1}, and 606 cm^{-1}) observed in the FTIR results. Additionally, the XRF results confirm the highest concentration of the inorganic compound CaO (11.634% w/w) in Cry–Ca–COS.

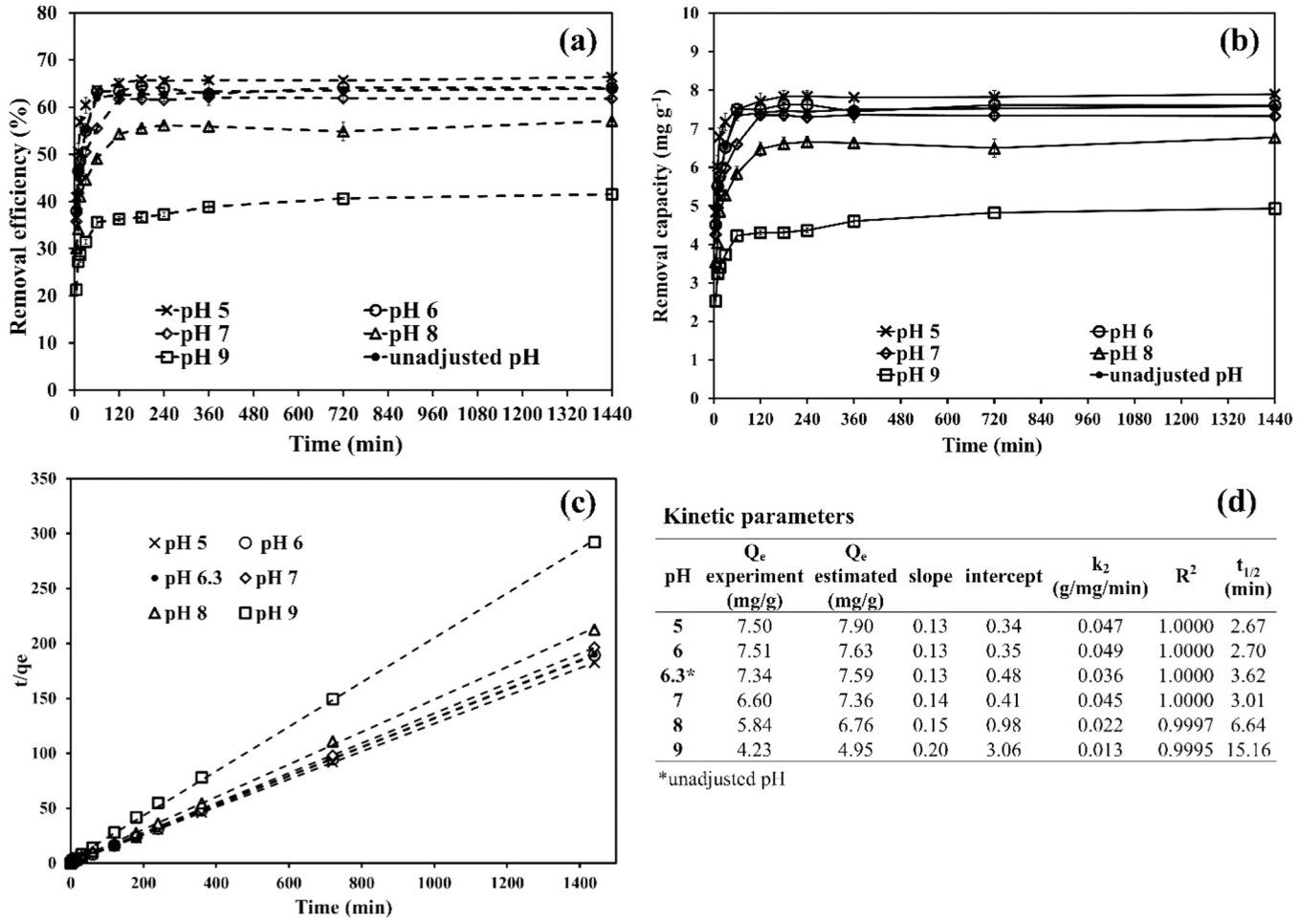

(d)

Kinetic parameters

pH	Q_e experiment (mg/g)	Q_e estimated (mg/g)	slope	intercept	k_2 (g/mg/min)	R^2	$t_{1/2}$ (min)
5	7.50	7.90	0.13	0.34	0.047	1.0000	2.67
6	7.51	7.63	0.13	0.35	0.049	1.0000	2.70
6.3*	7.34	7.59	0.13	0.48	0.036	1.0000	3.62
7	6.60	7.36	0.14	0.41	0.045	1.0000	3.01
8	5.84	6.76	0.15	0.98	0.022	0.9997	6.64
9	4.23	4.95	0.20	3.06	0.013	0.9995	15.16

*unadjusted pH

Fig. 7. Influences of the pH and contact time on (a) removal efficiency (%) (b) removal capacity of Cry–Ca–COS. Adsorption kinetics (c) and (d) kinetic parameters with the pseudo-second-order models at various pH. Conditions: 1 g Ca–COS in Cry–Ca–COS, phosphate concentration 12 mg L^{-1} for 1 L, temperature 25°C.

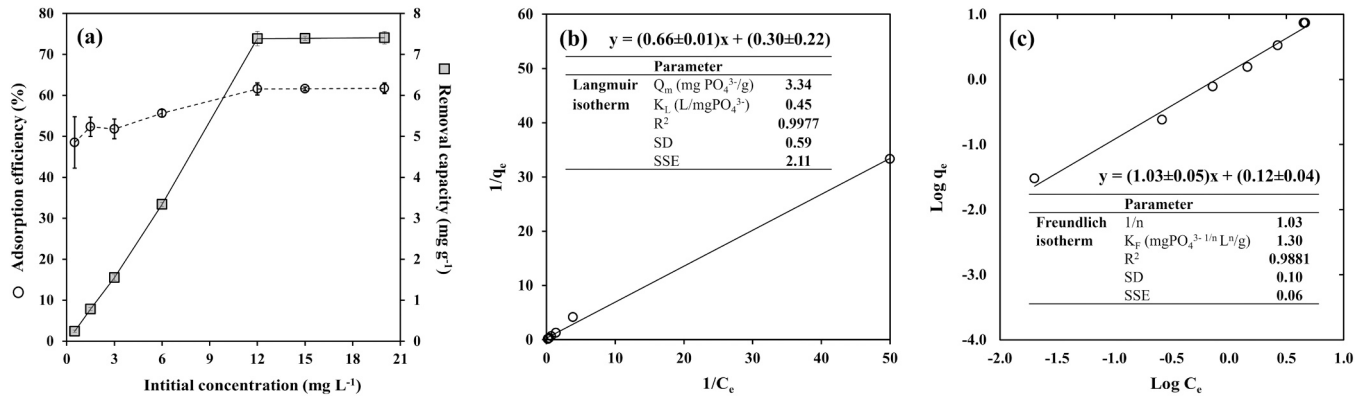

Fig. 8. (a) Influence of the initial phosphate concentration on the phosphate removal efficiency (%RE) and removal capacity of Cry–Ca–COS. Adsorption isotherms according to the (b) Langmuir model and (c) Freundlich model. Conditions: 1 g Ca–COS in Cry–Ca–COS, 1 L phosphate solution, without pH adjustment (pH 6.3), contact time 1 hour, temperature 25°C.

3.2. Phosphate adsorption on Cry–Ca–COS

3.2.1. Optimum amount of adsorbents

Fig. 6 illustrates the impact of Ca–COS dosage on the RE of phosphate. As the amount of Ca–COS increased from 0.5 to 1 g, the RE rose from 54.31% ± 0.52%–90.68% ± 1.61% (Fig. 6a), attributed to an augmentation in adsorption sites [14]. The RE remained constant even with further increases in Ca–COS quantity to 2.5–15 g. This constancy arises because an excessive amount of adsorbent can impede adsorption due to mass transfer resistance between the adsorbate and adsorbent, particularly within a confined space [20]. Additionally, a higher dose may lead to the aggregation of Ca–COS particles, resulting in a decrease in active surface area [50]. Similar patterns were observed for Cry–Ca–COS (Fig. 6b). Elevating the Ca–COS content from 0 to 2.5 g (0–2.5% w/w) increased the RE from 9.28% ± 0.84%–79.41% ± 0.52%, but further increases in Ca–COS content did not result in additional RE improvement. Cry–Ca–COS might necessitate more Ca–COS for phosphate adsorption due to the destruction of active sites caused by immobilization in the starch gel. This aligns with the BET results, which showed that Cry–Ca–COS had a lower surface area compared to Ca–COS. However, increasing the Ca–COS content from 1% to 2.5% w/w led to a decrease in the removal capacity (Qe) of Cry–Ca–COS from 7.38 ± 0.06–3.81 ± 0.03 mg g^{-1}. Consequently, 1 g of Ca–COS was added to 10 g of gel precursor (1% w/w) for further investigation of Cry–Ca–COS. Cry without Ca–COS adsorbed phosphate with a RE of 9.28% ± 0.84%, attributable to the presence of crosslinked Ca^{2+} in its structure, similar to what has been reported for a CSH composite [16].

3.2.2. Influence of pH

The impact of pH on the RE of Cry–Ca–COS was investigated by adjusting the pH of the standard phosphate solution within the range of 5.0–9.0 using small volumes of 0.1 M HCl or 0.1 M NaOH. However, the solution's pH (final pH) changed after phosphate adsorption at equilibrium time (60 minutes) from pH 6.9–10.2. This shift was due to a higher concentration of OH^- dissociated from $Ca(OH)_2$, a major constituent of pyrolyzed oyster shells [19], and excess limewater used during the cryogel preparation. With increasing pH, the RE (Fig. 7a) and removal capacity (Fig. 7b) of Cry–Ca–COS decreased, a trend associated with the charge on the material surface and the physicochemical behavior of phosphate in water within this pH range. The investigation of the point of zero charge (pHpzc) (described on supplementary material S4) found that pHpzc was approximately 6.8; consequently, a positive charge on the adsorbent surface was expected when the pH of the phosphate solution was below 6.8 [51]. As $H_2PO_4^-$ and HPO_4^{2-} are the predominant phosphate anions in this pH range [52], higher phosphate RE was achieved at lower initial pH due to electrostatic attraction between the positively charged adsorbent surface and negatively charged phosphate ions. Since the difference in phosphate removal efficiencies at pH 5 (63.59% ± 0.16%) and pH 6.3 (without adjustment, a typical effluent pH [53], 62.11% ± 0.95%) was only −2.33%, no pH adjustment was chosen to potentially save costs in real applications.

3.2.3. Influence of competing ions

Potential interfering ions, including Cl^-, SO_4^{2-}, and NO_3^- ions (10 mM), were mixed with phosphate (85 nM) before the adsorption procedure to investigate their influence on the RE of Cry–Ca–COS. The phosphate RE remained at 61.08% ± 0.45% (a −0.75% change), demonstrating the strong phosphate selectivity of Cry–Ca–COS. Carbonate ions (CO_3^{2-}) were mixed with phosphate separately from the other anions due to their potential to restrict phosphate adsorption [10,16,17]. The results showed that adding CO_3^{2-} decreased the phosphate RE to 44.97% ± 0.77% (a −26.9% change), attributed to the formation of $CaCO_3$ instead of calcium phosphate precipitate [54]. It is worth noting that the concentration of CO_3^{2-} tested in this experiment (10 mM) is higher than that of phosphate (85 nM) by more than 100 times.

3.2.4. Influence of the initial concentration and adsorption isotherms

The initial phosphate concentration ranged from 0.5 to 20 mg L^{-1}, aligning with the typical measurement range of discharge wastewater [19]. This variation aimed to explore its impact on the RE of Cry–Ca–COS during a 1-hour batch adsorption. Elevating the initial concentration from 0.5 to 12 mg L^{-1} resulted in a rise in RE from 48.50% ± 6.26%–61.54% ± 1.47%. However, further increments did not yield additional improvements in RE (Fig. 8a). A similar trend manifested for the Qe, which peaked at 7.38 ± 0.85 mg g^{-1} at 12 mg L^{-1}, remaining constant thereafter. This suggests a diminishing adsorption performance at higher phosphate concentrations, mirroring observations in calcined oyster-shell studies [19]. This phenomenon was attributed to the depletion of binding sites, linked to an increased number of phosphates available for adsorption [19].

The experimental data were subjected to fitting with the Langmuir (Fig. 8b) and Freundlich (Fig. 8c) models. The Langmuir model provided a superior fit ($R^2 = 0.9977$), implying a monolayer surface coverage of phosphate on Cry–Ca–COS through chemisorption. The dimensionless constant (R_L), as calculated by Equation (15) [9,10], ranged from 0.33 to 0.99, indicating favorable adsorption conditions ($0 < R_L < 1$). Some studies have proposed a dual mechanism where phosphate can both adsorb and precipitate on Ca–COS when pyrolysis fails to produce fully activated CaO [19,55]. For Cry–Ca–COS, a dual mechanism is plausible, as evidenced by suspended solids observed post-adsorption experiments, pointing to the formation of calcium phosphate precipitate through homogeneous and/or heterogeneous nucleation [19,55], in addition to phosphate adsorption on the surface.

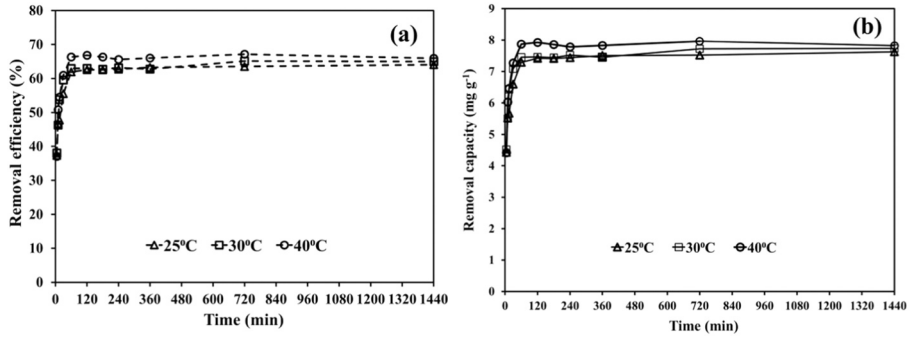

(c)

Thermodynamic parameters

Temperature (K)	ΔG° (kJ/mol)	ΔH° (kJ/mol)	ΔS° (J/mol/K)
298	-1.26	9.3	35.4
303	-1.43		
313	-1.79		

Fig. 9. Influences of the temperature and contact time on (a) the phosphate removal efficiency (%) and (b) removal capacity of Cry–Ca–COS. Adsorption thermodynamic parameters (c). Conditions: 1 g Ca–COS in Cry–Ca–COS, phosphate concentration 12 mg L^{-1} for 1 L, without pH adjustment (pH 6.3).

3.2.5. *Influence of contact time and adsorption kinetics*

The impact of contact time on the phosphate adsorption of Ca–COS and Cry–Ca–COS was investigated over a period of 0–1440 minutes (Fig. 7). Ca–COS exhibited a rapid increase in RE, reaching 73.44% ± 0.42% within 5 minutes and stabilizing at 90.04% ± 1.13% within 30 minutes. This trend aligns with findings in pyrolyzed materials [19,20,55] and suggests a potential phosphate adsorption mechanism involving chemical surface precipitation [19,42] or superior physicochemical adsorption depending on specific surface properties [34]. In contrast, Cry–Ca–COS exhibited a slower phosphate removal rate, with an RE of 37.28% ± 0.95% at 5 minutes, rising to 62.11% ± 0.95% within 60 minutes and only slightly increasing to 63.91% ± 0.79% after 1440 minutes (Fig. 7a, pH = 6.3). Similar to other polymer composites such as Cry-CSH [16] and PVA-CSH [13], the polymer matrix in Cry–Ca–COS may contribute to a decreased adsorption rate, leading to a prolonged equilibration period. The removal capacity of Cry–Ca–COS saw a rapid increase from 4.42 ± 0.11–7.34 ± 0.13 mg g^{-1} within 60 minutes, with no significant increase beyond that period (Fig. 7b). The decrease in adsorption rate over time may be attributed to the reduction of vacant sites on the Cry–Ca–COS surface [20], making it difficult for phosphate to occupy the remaining sites due to repulsive forces from the bulk phase [56].

Experimental results were fitted to the pseudo-first-order and pseudo-second-order kinetic models, with the latter providing a superior fit ($R^2 = 0.9995$) (Fig. 7c). This suggests that phosphate adsorption onto Cry–Ca–COS occurs via chemisorption, consistent with findings in CSH composite polymers [13,16]. The value of k_2 showed a slight increase from 0.047 to 0.049 g mg^{-1} min^{-1} with an adjusted pH increase from pH 5 to pH 6, leveling off at pH 7–9 (k_2 at pH 9 = 0.013 g mg^{-1} min^{-1}) (Fig. 7d). This was attributed to electrostatic repulsion between the negatively charged Cry–Ca–COS surface and $H_2PO_4^-$ and HPO_4^{2-} within the pH range. In contrast, k_2 increased from 0.031 to 0.133 g mg^{-1} min^{-1} with a temperature increase from 25°C to 40°C, indicating an endothermic nature of the phosphate removal process. The estimated Qe at unadjusted pH was 7.59 mg g^{-1}, closely aligning with the experimental data value of 7.34 ± 0.13 mg g^{-1}. The half-life time $t_{1/2}$, representing the time needed to adsorb 50% of phosphate at equilibrium, increased with rising pH (2.67–15.16 minutes at pH 5 to pH 9), confirming slower adsorption kinetics when pH > pHpzc. Conversely, $t_{1/2}$ decreased from 4.28 to 0.96 minutes with a temperature increase from 25°C to 40°C, indicating faster adsorption kinetics at higher temperatures—beneficial for practical use in tropical countries like Thailand.

3.2.6. *Influence of temperature and adsorption thermodynamic*

The impact of temperature on phosphate adsorption using Cry–Ca–COS was investigated within the temperature range of 25°C to 40°C. Both the RE (Fig. 9a) and removal capacity (Fig. 9b) exhibited an increase with temperature, suggesting an endothermic adsorption process akin to that observed in pyrolyzed eggshells [20]. The calculated activation energy (Ea) for phosphate adsorption on Cry–Ca–COS, using Equation (17), was determined to be 81.9 kJ mol^{-1}. This high value indicates a chemical adsorption process (Ea > 40 kJ mol^{-1}) rather than a physical adsorption process (Ea < 40 kJ mol^{-1}). The reduction in the negative ΔG° (Fig. 9c) signifies a more favorable and spontaneous adsorption of phosphate on Cry–Ca–COS at higher temperatures. The positive value of ΔH° confirms the endothermic nature of the adsorption process, while the positive value of ΔS° indicates an increase in the degree of disorder and randomness at the solid–solution interface during the adsorption process. This phenomenon is attributed to the interaction of phosphate with the active sites of the adsorbent, leading to the formation of stable structures.

3.2.7. *Influence of Cry–Ca–COS thickness*

The monolithic Cry–Ca–COS, prepared with dimensions of 2.5 cm thickness × 7.0 cm diameter, was divided into tablets of varying thickness to observe their impact on phosphate adsorption. When the Cry–Ca–COS was split into three thinner pieces (0.83 cm thickness each), a higher RE of 83.11% ± 0.68% was achieved compared to splitting it into two thicker pieces (1.25 cm thickness), resulting in an RE of 71.33% ± 0.95%. This difference was attributed to the increased number of active sites that phosphate could access. Consequently, the adsorbent was fashioned into tablets with a thickness of 0.83 cm, and three tablets were employed in the batch adsorption of 1 L of phosphate solution.

3.3. *Real sample application*

Cry–Ca–COS was employed for the recovery of phosphate in five real water samples: one influent wastewater sample, two effluent samples from a municipal treatment plant, and two surface water samples collected from the Pak Bang Canal in Patong, Phuket, Thailand. Initial measurements using the method described above revealed phosphate concentrations in the samples ranging from 1.05 ± 0.01–1.77 ± 0.01 mg L^{-1}. Through batch adsorption using three pieces of Cry–Ca–COS with a thickness of 0.83 cm, phosphate concentrations were effectively lowered to a range of 0.17 ± 0.01–0.29 ± 0.01 mg L^{-1}, yielding removal efficiencies (RE) between 83.40% ± 0.48% and 84.75% ± 0.40%. When employing 5 pieces of Cry–Ca–COS, phosphate concentrations were reduced to levels below those capable of inducing eutrophication (0.02 mg L^{-1} [9,10]), demonstrating remarkable RE within the range of 98.48% ± 1.87%–99.16% ± 0.72%. After adsorption, chemical oxygen demand (COD) in the samples increased, accompanied by a rise in total soluble solids (TSS), attributed to calcium phosphate precipitation. However, these increments remained below the established maximum guidelines for discharge from municipal wastewater treatment plants in Thailand (COD ≤ 120 mg L^{-1}, TSS ≤ 50 mg L^{-1}) [57]. This was consistent even after adsorption by Ca–COS, showcasing RE ranging from 87.71% ± 0.67%–89.92% ± 0.72%.

Cry–Ca–COS samples, following phosphate adsorption, were buried in soil (collected from the geographic location: latitude

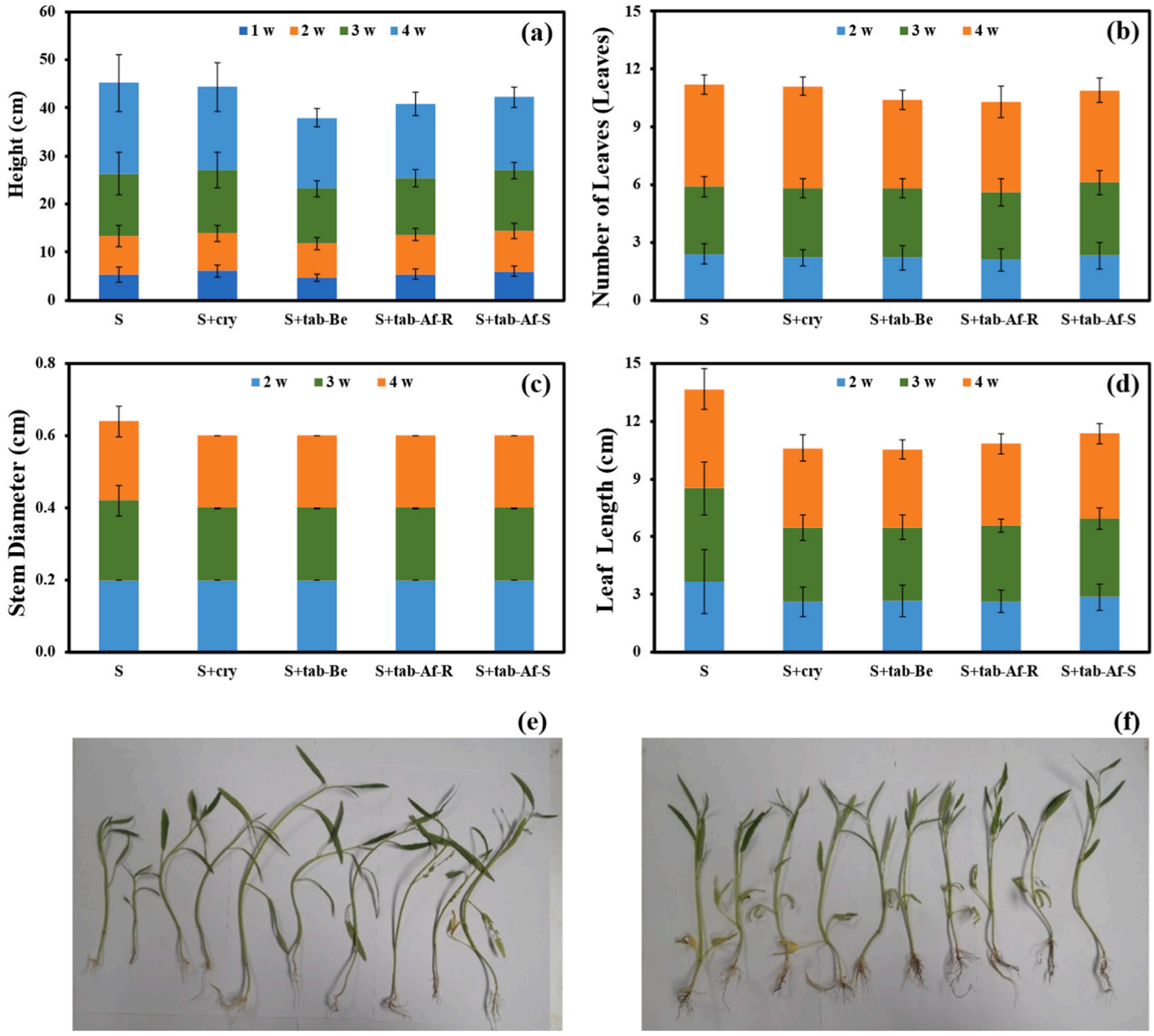

Fig. 10. Preliminary results of plant growth after 4 weeks under various soil conditions, including: control soil (S), soil with cryogel tablet without Ca–COS (S+cry), soil with Cry–Ca–COS tablet before phosphate adsorption (S+tab-Be), soil with Cry–Ca–COS after phosphate adsorption from real samples (S+tab-Af-R), and after standard phosphate adsorption (S+tab-Af-S). The results cover (a) height, (b) number of leaves, (c) stem diameter, and (d) leaf length. Images of morning glory after 4 weeks of growth using (e) S, and (f) S+tab-Af-R are included.

Table 1
Total and root length, fresh and dried weight of morning glory grown in various soil conditions for 4 weeks.

Sample	Total length (cm)	Root length (cm)	Fresh Weight (g)	Dried Weight (g)
S	23.45±7.36	4.60±1.78	0.70±0.37	0.08±0.02
S+cry	21.75±5.11	4.55±0.80	0.55±0.18	0.05±0.02
S+tab-Be	20.25±2.54	5.55±1.09	0.54±0.14	0.06±0.01
S+tab-Af-R	21.50±2.41	6.05±1.19	0.55±0.10	0.06±0.01
S+tab-Af-S	21.30±2.25	6.10±1.45	0.66±0.13	0.06±0.01

S: control soil; S+cry: soil with cryogel tablet without Ca–COS; S+tab-Be: soil with Cry–Ca–COS tablet before phosphate adsorption; S+tab-Af-R: soil with Cry–Ca–COS after phosphate adsorption from real samples; S+tab-Af-S: soil with Cry–Ca–COS after standard phosphate adsorption.

7.892369872431756 and longitude 98.3504886874602) to examine their biodegradability. Within 24 days, the Cry–Ca–COS samples exhibited a complete loss of 100% of their weight, attributed to hydrolysis and microbial activity [16]. It has been reported that starch can be invaded by bacteria, fungi, and other microorganisms under appropriate conditions in soil, which is a complex ecosystem containing various microorganism communities [58]. These findings affirm the biodegradable nature of Cry–Ca–COS. The material not only effectively adsorbs phosphate from contaminated water samples but can also be buried, releasing the phosphate back into the soil as a fertilizer for plants.

A preliminary study was conducted to explore the feasibility of utilizing phosphate-adsorbed Cry–Ca–COS as a fertilizer for cultivating water spinach (*Ipomoea aquatica* Forsk.), a rapidly growing vegetable popular in Thailand. Cryogel without Ca–COS (S+Cry), Cry–Ca–COS before (S+tab-Be), and after adsorption of phosphate from real samples

Table 2
The phosphate removal capacities of various bioadsorbents.

Adsorbent	Form of adsorbent	Removal capacity (mg g^{-1})	Removal efficiency (%)	Time (min)	Temperature (K)	Reference
Eggshell ash	Fine particle	121	80	120	323.15	[20]
Mussel shell	Fine particle	–	95	5	–	[55]
Palygorskite	Fine particle	4	–	120	298.15	[60]
Industrial waste	Fine particle	24.1	–	480	318.15	[14]
Cry–Ca–COS	Composite tablet	9.97	83.11	60	298.15	This work

(S+tab-Af-R; approximately 17 mg PO_4^{3-}) and phosphate standard (S+tab-Af-S; approximately 16 mg PO_4^{3-}) (7 pieces for each pot) were buried in soil (13 g) for 1 month to allow complete biodegradation. Five planting pots, including control soil (soil without additional material; S), were used to plant water spinach using the same procedure, and growth parameters were investigated for 4 weeks [59]. The results indicated that the height (Fig. 10a), leaf number (Fig. 10b), and stem diameter (Fig. 10c) of the plants growing in S+tab-Af-R and S+tab-Af-S pots showed no significant difference compared to the control soil (S) (t-calculated = 0.92–2.09, t-critical = 2.30), while the control pot provided longer leaves than others (Fig. 10d). The average total length (including root length), root length, fresh weight, and dried weight of 10 morning glories grown for 4 weeks in each pot are shown in Table 1, while images of the plants from control pot and the S+tab-Af-R pot are presented in Fig. 10e and f, respectively. As the growth of the plant is influenced by various parameters such as the type of plant, nutrient availability, pH, etc., further in-depth investigation is underway for a comprehensive report.

Thus, Cry–Ca–COS is an environmentally friendly attractive option for phosphate removal and recovery with a performance comparable to that of other biomaterials (Table 2). It is evident that the removal efficiency of the Cry–Ca–COS developed in this work is comparable to that of other biomaterials, while its removal capacity exceeds that of palygorskite [60] but falls short of the capacity demonstrated by fine particles derived from eggshell ash and industrial waste, which require longer contact time. However, it is worth noting that its tablet form can reduce material loss during operation, facilitate its recovery, and has a feasibility to be used as fertilizer for plant directly. While it's acknowledged that increasing contact time and temperature could enhance removal capacity, it's essential to consider potential increases in operational costs.

4. Conclusion

Cry–Ca–COS emerges as an environmentally friendly adsorbent for the removal and recovery of phosphate from water, employing two mechanisms: chemisorption and precipitation. The cryogel matrix, distinguished by its larger size, prevents the loss of the adsorbent, facilitating easy recovery post-usage. Under optimal conditions, a maximum removal capacity of 9.97 mg g^{-1} was achieved, yielding a RE of 83.11% ± 0.68%. The experimental data aligned well with the Langmuir isotherm model and pseudo-second-order kinetic model, indicating a monolayer surface coverage of phosphate on Cry–Ca–COS through chemisorption. This concurs with the estimated activation energy of 81.9 kJ mol^{-1}. The positive enthalpy value (ΔH°, 9.3 kJ mol^{-1}) affirms the endothermic nature of the adsorption process, consistent with the heightened adsorption rate at elevated temperatures.

In real samples, Cry–Ca–COS demonstrated an impressive RE ranging from 98.48% ± 1.87%–99.16% ± 0.72%. Remarkably, it biodegraded within 24 days when buried in soil, suggesting its potential application in agriculture as a fertilizer. Being in tablet form, Cry–Ca–COS minimizes material loss and simplifies the removal process compared to adsorbents in the form of fine particles. Given the escalating production of oyster shell waste in countries, including Thailand, recycling can alleviate its accumulation. Furthermore, the direct application of Cry–Ca–COS post-phosphate adsorption as fertilizer aligns with a zero-waste approach.

Declaration of Funding statement

This research was funded by the National Science, Research, and Innovation Fund (NSRF) and Prince of Songkla University (Grant No: TAE6601072d).

CRediT authorship contribution statement

Bussakorn Kleangklao: Visualization, Investigation, Data curation. **Tarawee Taweekarn:** Visualization, Data curation. **Chanita Boonkanon:** Visualization, Data curation. **Worawit Wongniramaikul:** Writing – review & editing, Validation, Resources, Methodology, Data curation, Conceptualization. **Satabodee Kaewnoo:** Validation, Methodology, Investigation, Data curation. **Aree Choodum:** Writing – review & editing, Writing – original draft, Validation, Supervision, Resources, Project administration, Methodology, Data curation, Conceptualization. **Diana Aga:** Writing – review & editing, Methodology, Conceptualization. **Chanadda Phawachalotorn:** Writing – review & editing, Validation, Methodology, Data curation. **Somsak Limwongsakorn:** Resources.

Declaration of Competing Interest

The authors declare that they have no known competing financial interests or personal relationships that could have appeared to influence the work reported in this paper.

Data Availability

Data will be made available on request.

Appendix A. Supporting information

Supplementary data associated with this article can be found in the online version at doi:10.1016/j.colsurfa.2024.133857.

References

[1] C. Alewell, B. Ringeval, C. Ballabio, D.A. Robinson, P. Panagos, P. Borrelli, Global phosphorus shortage will be aggravated by soil erosion, Nat. Commun. 11 (2020) 4546, https://doi.org/10.1038/s41467-020-18326-7.
[2] M.C. Chrispim, M. Scholz, M.A. Nolasco, Phosphorus recovery from municipal wastewater treatment: critical review of challenges and opportunities for developing countries, J. Environ. Manag. 248 (2019) 109268, https://doi.org/10.1016/j.jenvman.2019.109268.
[3] D. Cordell, S. White, Tracking phosphorus security: indicators of phosphorus vulnerability in the global food system, Food Secur. 7 (2015) 337–350, https://doi.org/10.1007/s12571-015-0442-0.
[4] P. Panagos, J. Köningner, C. Ballabio, L. Liakos, A. Muntwyler, P. Borrelli, E. Lugato, Improving the phosphorus budget of European agricultural soils, Sci. Total Environ. 853 (2022) 158706, https://doi.org/10.1016/j.scitotenv.2022.158706.
[5] D. Cordell, S. White, Life's bottleneck: sustaining the world's phosphorus for a food secure future, Annu. Rev. Environ. Resour. 39 (2014) 161–188, https://doi.org/10.1146/annurev-environ-010213-113300.
[6] L. Reijnders, Phosphorus resources, their depletion and conservation, a review, Resour. Conserv. Recycl. 93 (2014) 32–49, https://doi.org/10.1016/j.resconrec.2014.09.006.

[7] M. Blackwell, T. Darch, R. Haslam, Phosphorus use efficiency and fertilizers: future opportunities for improvements, Front. Agr. Sci. Eng. 6 (2019) 332–340, https://doi.org/10.15302/j-fase-2019274.
[8] P. Cornel, C. Schaum, Phosphorus recovery from wastewater: needs, technologies and costs, Water Sci. Technol. 59 (2009) 1069–1076, https://doi.org/10.2166/wst.2009.045.
[9] I.W. Almanassra, V. Kochkodan, M. Subeh, G. McKay, M. Atieh, T. Al-Ansari, Phosphate removal from synthetic and treated sewage effluent by carbide derive carbon, J. Water Process Eng. 36 (2020) 101323, https://doi.org/10.1016/j.jwpe.2020.101323.
[10] M.K. Seliem, S. Komarneni, M.R. Abu Khadra, Phosphate removal from solution by composite of MCM-41 silica with rice husk: Kinetic and equilibrium studies, Microporous Mesoporous Mater. 224 (2016) 51–57, https://doi.org/10.1016/j.micromeso.2015.11.011.
[11] I.W. Almanassra, V. Kochkodan, G. McKay, M.A. Atieh, T. Al-Ansari, Review of phosphate removal from water by carbonaceous sorbents, J. Environ. Manag. 287 (2021) 112245, https://doi.org/10.1016/j.jenvman.2021.112245.
[12] I.W. Almanassra, G. McKay, V. Kochkodan, M. Ali Atieh, T. Al-Ansari, A state of the art review on phosphate removal from water by biochars, Chem. Eng. J. 409 (2021) 128211, https://doi.org/10.1016/j.cej.2020.128211.
[13] S. Ding, D. Fang, Z. Pang, B. Luo, L. Kuang, H. Wang, Q. Zhang, Q. Shen, F. Ji, Immobilization of powdery calcium silicate hydrate via PVA covalent cross-linking process for phosphorus removal, Sci. Total Environ. 645 (2018) 937–945, https://doi.org/10.1016/j.scitotenv.2018.07.197.
[14] R. Xie, Y. Chen, T. Cheng, Y. Lai, W. Jiang, Z. Yang, Study on an effective industrial waste-based adsorbent for the adsorptive removal of phosphorus from wastewater: equilibrium and kinetics studies, Water Sci. Technol. 73 (2016) 1891–1900, https://doi.org/10.2166/wst.2016.021.
[15] K. Okano, S. Miyamaru, Y. Yamamoto, M. Kunisada, H. Takano, M. Toda, K. Honda, H. Ohtake, A mobile pilot-scale plant for in situ demonstration of phosphorus recovery from wastewater using amorphous calcium silicate hydrates, Sep. Purif. Technol. 170 (2016) 116–121, https://doi.org/10.1016/j.seppur.2016.06.040.
[16] T. Taweekarn, W. Wongniramaikul, A. Choodum, Removal and recovery of phosphate using a novel calcium silicate hydrate composite starch cryogel, J. Environ. Manag. 301 (2022) 113923, https://doi.org/10.1016/j.jenvman.2021.113923.
[17] Z. Zhang, X. Wang, J. Zhao, Phosphate recovery from wastewater using calcium silicate hydrate (C-S-H): sonochemical synthesis and properties, Environ. Sci.: Water Res. Technol. 5 (2019) 131–139, https://doi.org/10.1039/C8EW00643A.
[18] D. Frau, M.E. Spies, Y. Battauz, J. Medrano, R. Sinistro, Approaches for phosphorus removal with calcium hydroxide and floating macrophytes in a mesocosm experiment: impacts on plankton structure, Hydrobiologia 828 (2019) 287–299, https://doi.org/10.1007/s10750-018-3819-1.
[19] M.C. Martins, E.B.H. Santos, C.R. Marques, First study on oyster-shell-based phosphorous removal in saltwater — a proxy to effluent bioremediation of marine aquaculture, Sci. Total Environ. 574 (2017) 605–615, https://doi.org/10.1016/j.scitotenv.2016.09.103.
[20] J. Torit, D. Phihusut, Phosphorus removal from wastewater using eggshell ash, Environ. Sci. Pollut. Res. 26 (2019) 34101–34109, https://doi.org/10.1007/s11356-018-3305-3.
[21] S.Z.N. Ahmad, R. Hamdan, A. Al-Gheethi, S. Alkhadher, N. Othman, Removal of phosphate from wastewater by steel slag with high calcium oxide column filter system; efficiencies and mechanisms study, J. Chem. Technol. Biotechnol. 95 (2020) 3232–3240, https://doi.org/10.1002/jctb.6501.
[22] W.H. Park, C. Polprasert, Roles of oyster shells in an integrated constructed wetland system designed for P removal, Ecol. Eng. 34 (2008) 50–56, https://doi.org/10.1016/j.ecoleng.2008.05.014.
[23] G.-L. Yoon, B.-T. Kim, B.-O. Kim, S.-H. Han, Chemical–mechanical characteristics of crushed oyster-shell, Waste Manag. 23 (2003) 825–834, https://doi.org/10.1016/S0956-053X(02)00159-9.
[24] C. Namasivayam, A. Sakoda, M. Suzuki, Removal of phosphate by adsorption onto oyster shell powder—kinetic studies, J. Chem. Technol. Biotechnol. 80 (2005) 356–358, https://doi.org/10.1002/jctb.1175.
[25] W.H. Park, C. Polprasert, Phosphorus adsorption characteristics of oyster shells and alum sludge and their application for nutrient control in constructed wetland system, J. Environ. Sci. Health, Part A 43 (2008) 511–517, https://doi.org/10.1080/10934520701796440.
[26] W.-T. Chen, C.-W. Lin, P.-K. Shih, W.-L. Chang, Adsorption of phosphate into waste oyster shell: thermodynamic parameters and reaction kinetics, Desalin. Water Treat. 47 (2012) 86–95, https://doi.org/10.1080/19443994.2012.696800.
[27] D.C. Seo, J.S. Cho, H.J. Lee, J.S. Heo, Phosphorus retention capacity of filter media for estimating the longevity of constructed wetland, Water Res. 39 (2005) 2445–2457, https://doi.org/10.1016/j.watres.2005.04.032.
[28] J.A. Currie, N.R. Harrison, L. Wang, M.I. Jones, M.S. Brooks, A preliminary study of processing seafood shells for eutrophication control, Asia-Pac. J. Chem. Eng. 2 (2007) 460–467, https://doi.org/10.1002/apj.82.
[29] C.W. Lee, H.B. Kwon, H.P. Jeon, B. Koopman, A new recycling material for removing phosphorus from water, J. Clean. Prod. 17 (2009) 683–687, https://doi.org/10.1016/j.jclepro.2008.11.019.
[30] K. Okano, S. Miyamaru, A. Kitao, H. Takano, T. Aketo, M. Toda, K. Honda, H. Ohtake, Amorphous calcium silicate hydrates and their possible mechanism for recovering phosphate from wastewater, Sep. Purif. Technol. 144 (2015) 63–69, https://doi.org/10.1016/j.seppur.2015.01.043.
[31] APHA-AWWA-WEF, Ascorbic acid method. In: Standard method for the examination of water and wastewater. American Public Health Association, Washington DC (1998).
[32] S. Sen Gupta, K.G. Bhattacharyya, Kinetics of adsorption of metal ions on inorganic materials: A review, Adv. Colloid Interface Sci. 162 (2011) 39–58, https://doi.org/10.1016/j.cis.2010.12.004.
[33] I. Langmuir, THE ADSORPTION OF GASES ON PLANE SURFACES OF GLASS, MICA AND PLATINUM, J. Am. Chem. Soc. 40 (1918) 1361–1403, https://doi.org/10.1021/ja02242a004.
[34] L. Peng, H. Dai, Y. Wu, Z. Dai, X. Li, X. Lu, Performance and adsorption mechanism of a magnetic calcium silicate hydrate composite for phosphate removal and recovery, Water Sci. Technol. 2017 (2018) 578–591, https://doi.org/10.2166/wst.2018.184.
[35] C. Boonkanon, K. Phatthanawiwat, L. Chuenchom, N. Lamthornkit, T. Taweekarn, W. Wongniramaikul, A. Choodum, Preparation and characterization of calcium cross-linked starch monolithic cryogels and their application as cost-effective green filters, Polym. (Basel) 13 (2021) 3975, https://doi.org/10.3390/polym13223975.
[36] A. Choodum, P. Kanatharana, W. Wongniramaikul, N. Nicdaeid, Poly vinyl alcohol cryogel as a selective test kit for pre and post blast trinitrotoluene, Sens. Actuators B: Chem. 222 (2016) 654–662, https://doi.org/10.1016/j.snb.2015.08.115.
[37] T. Taweekarn, W. Wongniramaikul, C. Boonkanon, C. Phanrit, W. Sriprom, W. Limsakul, W. Towanlong, C. Phawachalotorn, A. Choodum, Starch biocryogel for removal of methylene blue by batch adsorption, Polymers 14 (2022), https://doi.org/10.3390/polym14245543.
[38] M. Thommes, K. Kaneko, A.V. Neimark, J.P. Olivier, F. Rodriguez-Reinoso, J. Rouquerol, K.S.W. Sing, Physisorption of gases, with special reference to the evaluation of surface area and pore size distribution (IUPAC Technical Report), Pure Appl. Chem. 87 (2015) 1051–1069, https://doi.org/10.1515/pac-2014-1117.
[39] K.-W. Ma, H. Teng, CaO powders from oyster shells for efficient CO2 capture in multiple carbonation cycles, J. Am. Ceram. Soc. 93 (2010) 221–227, https://doi.org/10.1111/j.1551-2916.2009.03379.x.
[40] H.-B. Kwon, C.-W. Lee, B.-S. Jun, J.-d Yun, S.-Y. Weon, B. Koopman, Recycling waste oyster shells for eutrophication control, Resour., Conserv. Recycl. 41 (2004) 75–82, https://doi.org/10.1016/j.resconrec.2003.08.005.
[41] H.H.T. Vu, M.D. Khan, V.T. Tran, D.V. Quang, V.-D. Dao, S. Lee, J.W. Ahn, S.-h Jung, Use of Calcite Mud from Paper Factories in Phosphorus Treatment, Sustainability 12 (2020) 5982.
[42] K.C. Bal Krishna, M.R. Niaz, D.C. Sarker, T. Jansen, Phosphorous removal from aqueous solution can be enhanced through the calcination of lime sludge, J. Environ. Manag. 200 (2017) 359–365, https://doi.org/10.1016/j.jenvman.2017.06.003.
[43] W. Wongniramaikul, W. Limsakul, A. Choodum, A biodegradable colorimetric film for rapid low-cost field determination of formaldehyde contamination by digital image colorimetry, Food Chem. 249 (2018) 154–161, https://doi.org/10.1016/j.foodchem.2018.01.021.
[44] K. Yorseng, S. Siengchin, B. Ashok, A.V. Rajulu, Nanocomposite egg shell powder with in situ generated silver nanoparticles using inherent collagen as reducing agent, J. Bioresour. Bioprod. 5 (2020) 101–107, https://doi.org/10.1016/j.jobab.2020.04.003.
[45] B.-C. Liga, B. Natalija, Research of Calcium Phosphates Using Fourier Transform Infrared Spectroscopy, in: T. Theophile (Ed.), Infrared Spectroscopy, IntechOpen: Rijeka,, 2012.
[46] A. Destainville, E. Champion, D. Bernache-Assollant, E. Laborde, Synthesis, characterization and thermal behavior of apatitic tricalcium phosphate, Mater. Chem. Phys. 80 (2003) 269–277, https://doi.org/10.1016/S0254-0584(02)00466-2.
[47] S. Koutsopoulos, Synthesis and characterization of hydroxyapatite crystals: a review study on the analytical methods, J. Biomed. Mater. Res. 62 (2002) 600–612, https://doi.org/10.1002/jbm.10280.
[48] D. Siva Rama Krishna, A. Siddharthan, S.K. Seshadri, T.S. Sampath Kumar, A novel route for synthesis of nanocrystalline hydroxyapatite from eggshell waste, J. Mater. Sci.: Mater. Med. 18 (2007) 1735–1743, https://doi.org/10.1007/s10856-007-3069-7.
[49] J.-K. Han, H.-Y. Song, F. Saito, B.-T. Lee, Synthesis of high purity nano-sized hydroxyapatite powder by microwave-hydrothermal method, Mater. Chem. Phys. 99 (2006) 235–239, https://doi.org/10.1016/j.matchemphys.2005.10.017.
[50] N. Yeddou, A. Bensmaili, Equilibrium and kinetic modelling of iron adsorption by eggshells in a batch system: effect of temperature, Desalination 206 (2007) 127–134, https://doi.org/10.1016/j.desal.2006.04.052.
[51] F.A. Pavan, E.S. Camacho, E.C. Lima, G.L. Dotto, V.T.A. Branco, S.L.P. Dias, Formosa papaya seed powder (FPSP): preparation, characterization and application as an alternative adsorbent for the removal of crystal violet from aqueous phase, J. Environ. Chem. Eng. 2 (2014) 230–238, https://doi.org/10.1016/j.jece.2013.12.017.
[52] H. Dai, X. Tan, H. Zhu, T. Sun, X. Wang, Effects of commonly occurring metal ions on hydroxyapatite crystallization for phosphorus recovery from wastewater, Water 10 (2018) 1619.
[53] D. Fang, L. Huang, Z. Fang, Q. Zhang, Q. Shen, Y. Li, X. Xu, F. Ji, Evaluation of porous calcium silicate hydrate derived from carbide slag for removing phosphate from wastewater, Chem. Eng. J. 354 (2018) 1–11, https://doi.org/10.1016/j.cej.2018.08.001.
[54] C.W. Lee, H.B. Kwon, H.P. Jeon, B. Koopman, Phosphate recovery from water as hydroxyapatite with activated oystershell, Mater. Sci. Forum 486-487 (2005) 177–180, https://doi.org/10.4028/www.scientific.net/MSF.486-487.177.
[55] A. Abeynaike, L. Wang, M.I. Jones, D.A. Patterson, Pyrolysed powdered mussel shells for eutrophication control: effect of particle size and powder concentration

on the mechanism and extent of phosphate removal, Asia-Pac. J. Chem. Eng. 6 (2011) 231–243, https://doi.org/10.1002/apj.426.
[56] N.Y. Mezenner, A. Bensmaili, Kinetics and thermodynamic study of phosphate adsorption on iron hydroxide-eggshell waste, Chem. Eng. J. 147 (2009) 87–96, https://doi.org/10.1016/j.cej.2008.06.024.
[57] The Ministry of Natural Resources and Environment of Thailand, Notification of the Ministry of Natural Resources and Environment for Standard levels for Discharge from Municipal Wastewater Treatment Plant., T.M.o.N.R.a.E.o. Thailand, Editor. 2010.
[58] S. Jin, G. Yue, L. Feng, Y. Han, X. Yu, Z. Zhang, Preparation and properties of a coated slow-release and water-retention biuret phosphoramide fertilizer with superabsorbent, J. Agric. Food Chem. 59 (2011) 322–327, https://doi.org/10.1021/jf1032137.
[59] S. Pohan, The effect of organic fertilizers on growth and yield of water spinach (Ipomoea reptans Poir), JERAMI Indones. J. Crop Sci. 3 (2021) 37–44, https://doi.org/10.25077/jijcs.3.2.37-44.2021.
[60] H. Ye, F. Chen, Y. Sheng, G. Sheng, J. Fu, Adsorption of phosphate from aqueous solution onto modified palygorskites, Sep. Purif. Technol. 50 (2006) 283–290, https://doi.org/10.1016/j.seppur.2005.12.004.